

# Level Set Topology Optimization of Structures under Stress and Temperature Constraints

Sandilya Kambampati<sup>1</sup>

*University of California San Diego, San Diego, CA 92093, USA*

Justin S. Gray<sup>2</sup>

*NASA Glenn Research Center, Cleveland, OH 44135, USA*

H. Alicia Kim<sup>3</sup>

*University of California San Diego, San Diego, CA 92093, USA; Cardiff University, Cardiff, CF24 3AA, UK*

---

## Abstract

In this paper, we introduce a level set topology optimization formulation considering coupled mechanical and thermal loads. Examples considering stress and compliance minimization under temperature and volume constraints, and mass minimization under stress and temperature constraints, are presented. The p-norm of the stress field and temperature field is used to approximate the maximum stress and temperature, respectively. We show that the minimal compliant topologies under temperature constraints do not necessarily have low stress values, and the stress and temperature requirements can be conflicting. The results also show that designs obtained by ignoring the thermal or structural constraints can result in high values of temperature or stress, respectively, thus demonstrating the importance of using a coupled multi-physics model in the optimization.

---

<sup>1</sup>Postdoctoral Researcher, Structural Engineering, sakambampati@ucsd.edu

<sup>2</sup>Research Engineer, justin.s.gray@nasa.gov

<sup>3</sup>Jacobs Scholars Chair Professor, Structural Engineering, alicia@ucsd.edu

## 1. Introduction

This paper discusses topology optimization of load carrying heat dissipating devices, which may be used in aircraft structures to dissipate heat emanating from batteries, engines, or other heat generating sources [1]. The structures in high temperatures are prone to premature failure due to the combined thermo-mechanical loads. In addition, batteries, especially lithium-ion batteries can experience thermal runaway if the working temperature of the battery exceeds the limit. The design of such load carrying structures which can also dissipate heat, using level set topology optimization is the focus of this paper.

Topology optimization is an innovative and powerful tool used for optimizing structures in engineering design. The most popular topology optimization methods are density based methods, such as Solid Isotropic Material Penalization (SIMP) method [2], where the geometry is typically described by an element-wise constant distribution of material. Density based methods, however, do not have a clear definition for the boundary of the structure. The level set method, on the other hand, is a class of topology optimization methods that has a precise definition of the boundary. During optimization, the boundary is updated every iteration implicitly via the level set function, allowing for an easy treatment of topological changes such as merging and splitting holes. A comprehensive review of the level set methods for structural topology optimization can be found in [3].

Topology optimization of thermo-mechanical problems is challenging owing to the design-dependent nature of the thermal loading. Rodrigues and Fernandes [4] presented a material distribution approach to optimize the topology of a 2D solid subject to an increase in temperature. The compliance of the structure is minimized subject to a constraint on the volume. Xia and Wang [5] used the level set method to optimize the topology of a structure subject to an increase in temperature by minimizing the compliance subject to a volume constraint. Gao and Zhang [6] proposed the penalization of the thermal stress coefficient for topology optimization under thermo-elastic stress loads for minimum com-

pliance. The above studies found that the volume constraint could be inactive for such thermo-elastic topology optimization problems. Pedersen and Pedersen [7] argued that since compliance minimization causes inactivity of the volume constraint, it is not a useful objective function in thermo-elastic topology optimization problems. They instead proposed that optimizing for a uniform energy density is more useful, and showed that this objective function also was close to fulfilling strength maximization (stress minimization).

Stress-based design of thermal structures was presented by Deaton and Grandhi [8], where they explored different objective and constraint functions including mass minimization subject to a stress constraint. In [9], topology optimization was applied to design a 3D nozzle flap to minimize the compliance subject to constraints on the thermo-elastic stresses in specific areas of the domain. Takaloozadeh and Yoon [10] developed a topological derivative formulation for stress minimization problems considering thermo-elastic loading. In these studies, the temperature was assumed to be constant and independent of topology.

In reality, however, the temperature distribution of the structure is dependent on the design, in the presence of heat sources or heat sinks due to heat conduction inside the structure. Li et al. [11] presented the multi-objective optimization for uniform stress and heat flux distributions of a structure under a given mechanical and thermal loads. Kruijff et al. [12] studied the influence of heat conduction in both structural and material designs. Specifically, they presented a multi-objective topology optimization formulation, where two conflicting design criteria—the heat conduction and structural stiffness performances—were optimized. Gao et al. [13] optimized the topology of a structure with multiple materials under steady-state temperature and mechanical loading by minimizing the compliance subject to a mass constraint. More recently, Kang and James [14] presented multimaterial topology optimization with elastic and thermal response considerations. They conducted parallel uncoupled finite element analyses to simulate the elastic and thermal response of the structure. Zhu et al. [15] presented topology optimization of coupled thermo-mechanical

problems by minimizing the compliance of a structure subject to volume and temperature constraints.

Stress based design of structures considering heat conduction was discussed by Takezawa et al. [16]. The volume of a structure was minimized under the constraints of maximum stress and thermal compliance. Deng and Suresh [17] presented stress constrained topology optimization under mechanical loads and varying temperature fields. In [17], a topological sensitivity based level set method with an augmented Lagrangian method was developed to explore the Pareto topologies. However, topology optimization of thermo-mechanical structures considering heat conduction subject to both maximum temperature and stress constraints is not found in the literature. Constraining the maximum temperature of a structure is essential for a battery pack design, as high temperatures in the structure can trigger thermal runaway inside the batteries, which can be catastrophic. Such coupled multiphysics problems present a more challenging design space and the thermomechanical stress problems considering temperature constraints have not been successfully resolved in the field of topology optimization.

Consequently, in this study, we present level set topology optimization of structures under coupled mechanical and thermal loads considering stress and temperature constraints. The level set method is used for topology optimization, and the adjoint method is used to compute sensitivities. The effectiveness of the optimization method is demonstrated by designing an L-bracket and a battery pack under thermal and mechanical loading. We show that stress and temperature can be conflicting in optimization. Finally, we discuss the importance of including both stress and temperature constraints in the optimization process by showing that the designs obtained by ignoring the thermal or structural constraints can result in high values of temperature or stress, respectively. This clearly demonstrates that the optimum stress and temperature values obtained using a single-physics model are far from the optimum stress and temperature values obtained using the multi-physics model.

## 2. Optimization Method

The optimization algorithm presented in this study uses two separate grids: one to represent the level set function and one to conduct the finite element analyses for structural and heat transfer models. The boundary points and the volume fraction information computed by the level set function is passed on to the finite element analysis (FEA) mesh. The boundary velocities are optimized using the sensitivity values and mathematical programming, and are passed on to the level set grid. The level set function is updated based on the boundary point velocities by solving a Hamilton-Jacobi equation. In this section, the detailed descriptions of the mathematical models developed are presented.

### 2.1. Level Set Method

In the level set method, the boundary of the structure is described implicitly as [18]

$$\begin{aligned}\phi(x) &\geq 0, \quad x \in \Omega \\ \phi(x) &= 0, \quad x \in \Gamma \\ \phi(x) &< 0, \quad x \notin \Omega\end{aligned}\tag{1}$$

where  $\phi(x)$  is the implicit level set function,  $\Omega$  is the domain,  $\Gamma$  is the domain boundary. The boundary of the structure is changed under a given velocity field  $V_n(x)$  using the following Hamilton-Jacobi equation [19]

$$\frac{d\phi(x)}{dt} + |\nabla\phi(x)|V_n(x) = 0\tag{2}$$

The above equation is solved numerically using the following scheme:

$$\phi_i^{k+1} = \phi_i^k - \Delta t |\nabla\phi_i^k| V_{n,i}\tag{3}$$

where  $i$  is a discrete point in the domain,  $k$  is the iteration number, and  $|\phi_i|$  is computed using the Hamilton-Jacobi weighted essentially non-oscillatory (HJ-WENO [18]) scheme.

## 2.2. Heat transfer model description

The steady state heat equation [20] is used to model the heat transfer of a structure, given by

$$-\nabla \cdot (\kappa \nabla (\Delta T)) = Q \quad (4)$$

where  $\kappa$  is the conductivity coefficient,  $Q$  is the heat generation rate, and  $\Delta T = T - T_{ref}$  is the temperature difference from the reference temperature  $T_{ref}$ . The finite element analysis is used to solve the above equation in the discrete form

$$K_t t = q_t \quad (5)$$

where  $K_t$  is the conductivity matrix,  $q_t$  is the thermal load, and  $t$  is the temperature difference  $\Delta T$  computed on the finite element nodes.  $K_t$  is given by

$$K_t = \sum_{i=1}^{N_e} K_{ti}^e = \sum_{i=1}^{N_e} \kappa_i K_{t0}^e \quad (6)$$

where  $K_{ti}^e = \kappa_i K_{t0}^e$  is the thermal stiffness matrix of an element  $i$ ,  $N_e$  is the total number of finite elements, and  $K_{t0}^e$  is the homogeneous elemental thermal stiffness matrix given by

$$K_{t0}^e = \int_{\Omega_i} B^T B d\Omega \quad (7)$$

and

$$q_t = \sum_{i=1}^{N_e} q_{ti}^e = \sum_{i=1}^{N_e} \int_{\Omega_i} N^T Q d\Omega \quad (8)$$

where  $N$  is the shape functions, and the gradient  $B = \nabla N$  is the gradient of the shape functions,  $q_{ti}^e$  is the elemental thermal load,  $\Omega_i$  is the domain of an element  $i$ , and  $\kappa_i$  is the conductivity coefficient of the element  $i$ , given by

$$\kappa_i = \kappa_{min} + x_i(\kappa_0 - \kappa_{min}) \quad (9)$$

where  $x_i$  is the fraction of the elemental volume cut by the level set,  $\kappa_{min}$  is the conductivity coefficient of the passively conducting material, and  $\kappa_0$  is the conductivity coefficient of the solid material. The stiffness matrix  $K_t$  and the thermal load  $q_t$  are assembled using the above equations and Eq. 5 is solved to determine the temperature distribution.

### 2.3. Thermo-elastic model description

The temperature distribution causes the structure to expand or contract, resulting in thermal strain  $\epsilon_t$  due to thermo-elasticity. Specifically, the strain  $\epsilon_{t,i}$  of an element  $i$  caused by the temperature change is given as

$$\epsilon_{t,i} = \alpha_i t_i \quad (10)$$

where  $\alpha_i = x_i \alpha$  is the coefficient of the linear expansion of the element  $i$ ,  $\alpha$  is the coefficient of linear expansion of the solid material, and  $t_i$  is the temperature change of the element. The elemental strain is imposed on the element as an equivalent thermo-elastic force  $f_{ti}^e$ , given by [7]

$$f_{ti}^e = H_i^e t_i^e \quad (11)$$

where  $t_i^e$  is the temperature change at the nodes of an element  $i$ , and  $H_i^e$  is the elemental thermo-elastic force generating matrix given by

$$H_i^e = x_i H_0^e \quad (12)$$

where

$$H_0^e = \int_{\Omega_i} \alpha B_s^T C \epsilon^e N_s d\Omega \quad (13)$$

and  $B_s$  is the gradient of the displacement shape function matrix  $N_s$ ,  $C$  is the elasticity tensor, and  $\epsilon^e$  is the unit principal strain. The elemental thermo-elastic force is assembled to form the global thermo-elastic force  $f_t$  as

$$f_t = \sum_{i=1}^{N_e} f_{ti}^e = H t \quad (14)$$

where  $H$  is the matrix that assembles the thermo-elastic force from a given temperature distribution given by

$$H = \sum_i^{N_e} H_i^e \quad (15)$$

The thermo-elastic force is added to the mechanical force  $f_m$ , and the following equation is used to compute the displacement  $d$  under mechanical and thermal loads

$$K_s d = f_m + f_t = f_m + H t \quad (16)$$

where  $K_s$  is the structural stiffness matrix of the structure, given by

$$K_s = \sum_{i=1}^{N_e} K_{si}^e = \sum_{i=1}^{N_e} E_i K_{s0}^e \quad (17)$$

where  $K_{si}^e = E_i K_{s0}^e$  is the elemental stiffness matrix of an element  $i$ , and  $K_{s0}^e$  is the homogeneous elemental stiffness matrix, given by

$$K_{s0}^e = \int_{\Omega_i} B_s^T C B_s d\Omega \quad (18)$$

and  $E_i$  and  $E$  are the elasticity moduli of the element and the material, given by

$$E_i = E_{min} + (E - E_{min})x_i \quad (19)$$

where  $E_{min}$  is the elasticity modulus of the void.

#### 2.4. Optimization problem formulation

The objective of this study is to solve the following optimization problem

$$\begin{aligned} \min_{\Omega} \quad & J = \int_{\Omega} J(\Omega) d\Omega \\ \text{subject to} \quad & K_t t = q_t \\ & K_s d = f_m + H t \\ & G_j = \int_{\Omega} G_j(\Omega) d\Omega \leq g_j^0 \quad j = 1, 2, \dots, N_g, \end{aligned} \quad (20)$$

where  $J$  is an objective function,  $G_j$  is the  $j^{th}$  constraint function,  $g_j^0$  is the  $j^{th}$  constraint value, and  $N_g$  is the number of constraints. The objective function  $J$  and the constraint function  $G_j$  can be compliance, mass, stress, or temperature. The temperature state equations (Eq. 5) and the thermo-elastic state equations (Eq. 16) are included as equality constraints in the optimization formulation in Eq. 20.

For a given level set function topology, the objective and constraint functions are linearized using the boundary point sensitivities; and a sub-optimization problem is constructed using the sequential linear programming method for level set topology optimization [21]. The sub-optimization problem is solved using

the Simplex method [22], yielding the optimum boundary point velocities. The level set function is numerically updated using the boundary point velocities by solving Eq. 3. This process is repeated until convergence is obtained.

### 2.5. Sensitivity computation

In this section, the computations of the boundary point sensitivities for compliance, maximum stress, and maximum temperature, using the adjoint method are presented. First, the sensitivities are calculated at the centroids of all the elements from which the boundary point sensitivities are determined using the least squares interpolation [23].

#### 2.5.1. Compliance sensitivities

The compliance of the structure under thermal and mechanical loads is given by

$$C = d^T K_s d = f^T d = (f_m + Ht)^T d \quad (21)$$

The Lagrangian function  $\mathcal{L}$  of compliance is defined as

$$\mathcal{L} = (f_m + Ht)^T d + \lambda_d^T (f_m + Ht - K_s d) + \lambda_t^T (f_t - K_t t) \quad (22)$$

where  $\lambda_d$  and  $\lambda_t$  are the adjoint variables corresponding to structural displacement  $d$  and temperature  $t$ .  $\lambda_d$  is computed by solving  $\frac{\partial \mathcal{L}}{\partial d} = 0$ , which yields

$$f^T - \lambda_d^T K_s = 0 \quad (23)$$

Next,  $\lambda_t$  is computed by solving  $\frac{\partial \mathcal{L}}{\partial u} = 0$ , which yields

$$\lambda_d^T H - \lambda_t K_t = 0 \quad (24)$$

The Lagrangian function  $\mathcal{L}$  is differentiated with respect to the volume fraction  $x_i$  of each element to compute the elemental centroid sensitivities of compliance

$s_i$ , given by

$$\begin{aligned}
s_i &= \frac{\partial \mathcal{L}}{\partial x_i} \\
&= \frac{\partial}{\partial x_i} ((f_m + Ht)^T d + \lambda_d^T (f_m + Ht - K_s d) + \lambda_t^T (f_t - K_t t)) \\
&= t^T \frac{\partial H}{\partial x_i} d + \lambda_d^T \frac{\partial H}{\partial x_i} t - \lambda_d^T \frac{\partial K_s}{\partial x_i} d - \lambda_t^T \frac{\partial K_s}{\partial x_i} t \\
&= t_i^{eT} H_0^e d_i^e + \lambda_{di}^{eT} H_0^e t_i^e - \lambda_{di}^{eT} K_{s0}^e d_i^e - \lambda_{ti}^{eT} K_{t0}^e t_i^e
\end{aligned} \tag{25}$$

where  $\lambda_{di}^e$  and  $\lambda_{ti}^e$  are the adjoint variables of displacement and temperature at the element nodes, respectively,  $d_i^e$  and  $t_i^e$  are the displacement and temperature values at the nodes, respectively.

### 2.5.2. Maximum stress sensitivities

The maximum stress of a structure is approximated by the p-norm of the stress field which is given by

$$\sigma_p = \left( \sum_{i=1}^{N_e} \sigma_{p,i} \right)^{1/p} = \left( \sum_{i=1}^{N_e} \sum_{j=1}^{N_g} \sigma_{vm,ij}^p \right)^{1/p} \tag{26}$$

where  $\sigma_{vm,ij}$  is the von Mises stress of an element  $i$  at a Gauss point  $j$ ,  $N_e$  is the number of elements, and  $N_g$  is the number of Gauss points.  $\sigma_{vm,ij}$  is given by

$$\sigma_{vm,ij} = \sqrt{\sigma_{ij}^T V \sigma_{ij}} \tag{27}$$

where  $V$  is the Voigt matrix [24], and  $\sigma_{ij}$  is the stress tensor of an element  $i$  at a Gauss point  $j$ , given by

$$\sigma_{ij} = x_i C (B_{s,ij} d_i^e - \epsilon_{t,ij}) \tag{28}$$

where  $\epsilon_{t,ij} = B_{t,ij} t_i^e$  is the thermo-elastic strain, and

$$B_{t,ij} = \alpha \epsilon^e N_j \tag{29}$$

The Lagrangian function  $\mathcal{L}$  of the p-norm stress under the structural and thermal equilibrium is given by

$$\mathcal{L} = \sigma_p + \lambda_d^T (f_m + Ht - K_s d) + \lambda_t^T (f_t - K_t t) \tag{30}$$

The adjoint variable  $\lambda_d$  is computed by solving  $\frac{\partial \mathcal{L}}{\partial d} = 0$ , which yields

$$f_\sigma - \lambda_d^T K_s = 0 \quad (31)$$

where  $f_\sigma = \sum_i^{N_e} f_\sigma^i$  is the adjoint force computed by assembling the elemental adjoint forces  $f_\sigma^i$ , given by

$$\begin{aligned} f_\sigma^i &= \frac{\partial \sigma_{p,i}}{\partial d_i^e} \\ &= \frac{\partial}{\partial d_i^e} \left( \sum_{j=1}^{Ng} \sigma_{vm,ij}^p \right) \\ &= \frac{\sigma_p^{1-p}}{p} \sum_{j=1}^{Ng} p \sigma_{vm,ij}^{p-2} \sigma_{ij}^T VCB_{s,ij} \end{aligned} \quad (32)$$

The adjoint variable  $\lambda_t$  is computed by solving  $\frac{\partial \mathcal{L}}{\partial t} = 0$ , which yields

$$f_{\sigma,t} - \lambda_t^T K_t = 0 \quad (33)$$

where  $f_{\sigma,t} = \sum_i^{N_e} f_{\sigma,t}^i$  is the adjoint force computed by assembling the elemental adjoint forces  $f_{\sigma,t}^i$ , given by

$$\begin{aligned} f_{\sigma,t}^i &= \frac{\partial \sigma_{p,i}}{\partial t_i^e} \\ &= \frac{\partial}{\partial t_i^e} \left( \sum_{j=1}^{Ng} \sigma_{vm,ij}^p \right) \\ &= -\frac{\sigma_p^{1-p}}{p} \sum_{j=1}^{Ng} p \sigma_{vm,ij}^{p-2} \sigma_{ij}^T VCB_{t,ij} \end{aligned} \quad (34)$$

Next the Lagrangian function  $\mathcal{L}$  is differentiated with respect to the volume fraction of each element  $i$  to compute the sensitivities of the p-norm stress  $s_{\sigma,i}$ ,

given by

$$\begin{aligned}
s_{\sigma,i} &= \frac{\partial \mathcal{L}}{\partial x_i} \\
&= \frac{\partial}{\partial x_i} \left( \sigma_p + \lambda_d^T (f_m + Ht - K_s d) + \lambda_t^T (f_t - K_t t) \right) \\
&= \frac{\partial}{\partial x_i} \left( \sum_{i=1}^{N_e} \sum_{j=1}^{N_g} \sigma_{vm,ij}^p \right)^{1/p} + \lambda_d^T \frac{\partial H}{\partial x_i} t - \lambda_d^T \frac{\partial K_s}{\partial x_i} d - \lambda_t^T \frac{\partial K_s}{\partial x_i} t \\
&= \frac{\sigma_p^{1-p}}{p} \sum_{j=1}^{N_g} \left[ p \sigma_{vm,ij}^{p-2} \sigma_{ij}^T C(B_{s,ij} d_i^e - \epsilon_{t,ij}) \right] + \lambda_{di}^{eT} H_e^0 t_i^e - \lambda_{di}^{eT} K_{se}^0 d_i^e - \lambda_{ti}^{eT} K_{te}^0 t_i^e
\end{aligned}$$

The sensitivity of the maximum stress is then approximated as

$$s_i = \max_{\forall i,j} (\sigma_{vm,ij}) \frac{s_{\sigma,i}}{\sigma_p} \quad (36)$$

### 2.5.3. Temperature sensitivities

The maximum temperature of the structure is approximated using the p-norm of the temperature vector on the nodes. The p-norm  $T_p$  of the temperature is given by

$$T_p = \left( \sum_{i=1}^{N_n} t_i^p \right)^{1/p} \quad (37)$$

where  $N_n$  is the number of finite element nodes. The Lagrangian function  $\mathcal{L}$  of the temperature under the thermal equilibrium is given by

$$\mathcal{L} = T_p + \lambda_t^T (f_t - K_t t) \quad (38)$$

The adjoint variable  $\lambda_t$  is computed by solving  $\frac{\partial \mathcal{L}}{\partial t} = 0$ , which yields

$$\frac{T_p^{1-p}}{p} t^T - \lambda_t^T K_t = 0 \quad (39)$$

The Lagrangian function  $\mathcal{L}$  is differentiated with respect to the volume fraction of each element  $i$  to compute the elemental centroid sensitivities of the pnorm

of temperature  $s_{T,i}$ , given by

$$\begin{aligned}
s_{T,i} &= \frac{\partial \mathcal{L}}{\partial x_i} \\
&= \frac{\partial}{\partial x_i} (T_p + \lambda_t^T (f_t - K_t t)) \\
&= -\lambda_t^T \frac{\partial K_t}{\partial x_i} t \\
&= -\lambda_{ti}^{eT} K_{t0}^0 t_i^e
\end{aligned} \tag{40}$$

The sensitivity of the maximum temperature is computed as

$$s_i = \max_{\forall_i} (t_i) \frac{s_{T,i}}{T_p} \tag{41}$$

### 3. Numerical Examples

In this section, the numerical examples are presented. The compliance and stress of the structures are minimized under a volume constraint and a range of maximum temperature constraints. Next, the mass is minimized under stress and temperature constraints, and the resulting designs are compared. To the best of our knowledge, these examples, i.e., (a) the minimization of compliance and stress subject to volume and maximum temperature constraints and (b) minimization of mass subject to maximum stress and maximum temperature constraints are not found in literature. The sensitivity analysis presented in Sections 2.5.1, 2.5.2, and 2.5.3 for compliance, maximum stress, and maximum temperature, is used for the optimization. The first example is an L-bracket design, which is a classic benchmark problem for stress based topology optimization [25, 26, 27]. The L-bracket has a stress concentration at its re-entrant corner under the tip mechanical load. The objective is to design the structure by minimizing stress, thus effectively eliminating the re-entrant corner in the design. In this study, we augment the benchmark L-bracket problem by adding heat transfer physics to investigate the effects of thermal constraints in the optimized design. The next example is the design of a battery pack, which is commonly used in the design of electric aircraft such as the NASA's X-57

“Maxwell” aircraft [28]. We study the load-carrying and heat dissipating capability of light-weight optimized battery packs. From hereafter in the paper, unless otherwise mentioned, the word stress refers to von Mises stress.

### 3.1. L-bracket design

A schematic of an L-bracket (dimensions are  $0.1 \text{ m} \times 0.1 \text{ m}$  and a thickness of  $0.01 \text{ m}$ ) is shown in Figure 1. A square section of dimensions  $0.06 \text{ m} \times 0.06 \text{ m}$  is removed from the top-right side to form the L-bracket. The finite element mesh of size  $100 \times 100$  elements is used. A force  $F = 5 \text{ kN}$  is applied on the right hand side and the L-bracket is clamped on the top. A thermal load  $Q = 1.38 \text{ W}$  is applied on the right hand side and the top portion acts as a heat sink with  $T = 20 \text{ }^\circ\text{C}$ . The elastic modulus of the structure (titanium) is  $E = 120 \text{ GPa}$  with Poisson’s ratio  $\nu = 0.36$ , density  $\rho = 4500 \text{ kg/m}^3$ , and thermal conductivity  $\kappa = 20 \text{ W/m/}^\circ\text{C}$ . The reference temperature used is  $T_{ref} = 20 \text{ }^\circ\text{C}$ .

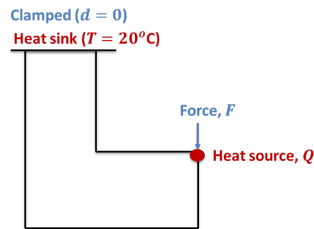


Figure 1: A schematic of an L-bracket subject to mechanical and thermal loading.

#### 3.1.1. Stress minimization

In this section, the p-norm stress  $\sigma_p$  of the L-bracket is minimized subject to a volume constraint  $V_0 \leq 50\%$  of the L-shaped design domain and the maximum temperature  $T^*$  constraints ranging from  $70 \text{ }^\circ\text{C}$  to  $90 \text{ }^\circ\text{C}$ . The value of  $p = 12$

is used in this study. The optimization problem can be described as

$$\begin{aligned}
 & \min_{\Omega} && \sigma_p \\
 \text{subject to} &&& K_t t = q_t \\
 &&& K_s d = f_m + H t \\
 &&& V \leq V_0 \\
 &&& T \leq T^*
 \end{aligned} \tag{42}$$

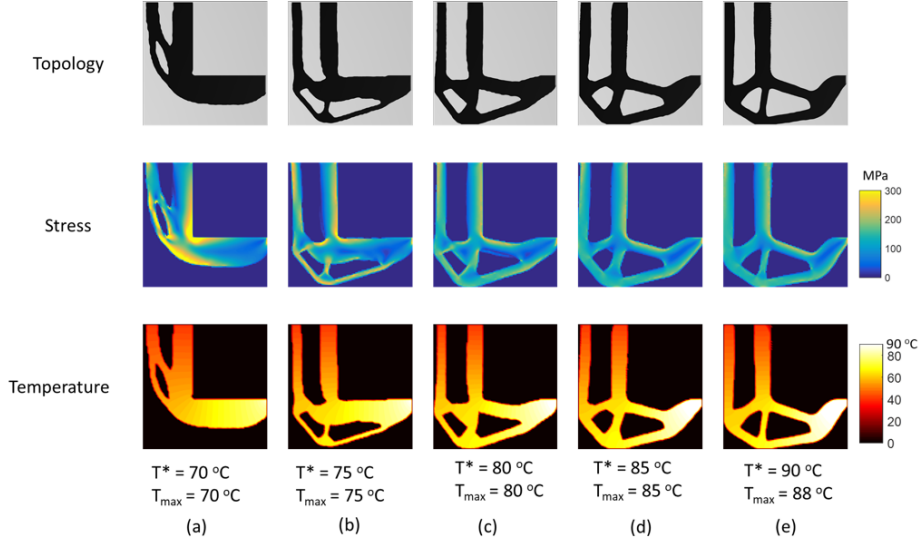


Figure 2: Optimal topologies, and the corresponding stress and temperature distributions obtained by minimizing the p-norm stress subject to a volume constraint of 50% and a range of maximum temperature constraints. The stress plots are clipped at 300 MPa.

Figure 2 shows the optimal topologies, their stress and temperature distributions obtained by minimizing the p-norm stress for varying maximum temperature constraints, and the actual maximum temperature of the structure  $T_{max}$ . The corresponding p-norm stress and the maximum stress values are shown in Figure 3. In Figure 2a, the optimized design for a temperature constraint of  $T^* = 70\text{ }^\circ\text{C}$  is shown, where we can see that the optimum design has a sharp re-entrant corner. For such low values of temperature constraint, the optimizer

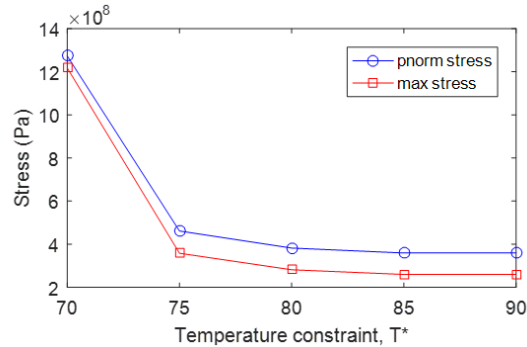


Figure 3: Optimal p-norm stress and corresponding maximum stress obtained by minimizing the p-norm stress subject to a volume constraint of 50% and a range of maximum temperature constraints.

tries to minimize the thermal load path distance from the heat source to the heat sink. Therefore the optimum design has material along the right angle of the L-bracket, retaining the sharp re-entrant corner, so as to minimize the thermal load path distance. As a result of the sharp re-entrant corner the maximum stress of the structure is high (greater than 1000 MPa).

In Figure 2b the optimized design for a temperature constraint of  $T^* = 75$  °C is shown. We can see that the optimum design has a slightly rounded off re-entrant corner compared to the optimum topology for  $T^* = 70$  °C (Figure 2a). This is because for  $T^* = 75$  °C, the optimized design need not have the shortest load path distance from the heat source to the heat sink. Therefore, the optimizer can now slightly round off the re-entrant corner and distribute material such that the stress is reduced while satisfying the temperature constraint. The maximum stress in the structure is now decreased from over 1000 MPa to approximately 400 MPa.

In Figures 2c to 2e, the optimized design for a temperature constraint of  $T^* = 80$  °C to  $T^* = 90$  °C is shown. As the maximum temperature constraint is relaxed, the optimizer has more freedom to distribute material so as to further minimize the stress. As a result, the topology gets wider and more rounder near the re-entrant corner and the maximum stress is reduced. The maximum stress

for all three cases in Figures 2c to 2e is approximately 300 MPa. Furthermore, the temperature constraint is active in all the cases except for when  $T^* = 90$  °C, with the maximum temperature  $T_{max} = 88$  °C (Figure 2e).

In conclusion, from Figures 2 and 3, we can see that for low values of temperature constraint, the optimizer retains the re-entrant corner to satisfy the temperature constraint, resulting in high values of stresses. As the temperature constraint is relaxed, the optimizer rounds off the re-entrant corner, resulting in lower stress values. Specifically the maximum stress is reduced from over 1000 MPa to approximately 300 MPa, when the temperature constraint is increased from 70 °C to 90 °C.

### 3.1.2. Compliance minimization

In this section, the designs are optimized by minimizing compliance instead of stress. We contrast the designs obtained by minimizing the compliance with the designs obtained by minimizing the stress. Specifically, the compliance  $C$  of the L-bracket is minimized subject to a volume constraint  $V_0 = 50\%$  and maximum temperature  $T^* = 80$  °C. The optimization problem can be described as

$$\begin{aligned} \min_{\Omega} \quad & C \\ \text{subject to} \quad & K_t t = q_t \\ & K_s d = f_m + H t \\ & V \leq V_0 \\ & T \leq T^* \end{aligned} \tag{43}$$

$$\tag{44}$$

Figure 4a shows the optimal topology and the corresponding stress and temperature distributions obtained by minimizing compliance. For the sake of comparison, we show in Figure 4b the optimum topology and the corresponding stress and temperature distributions obtained by minimizing stress for the same set of constraints. From Figure 4a, we can see that the optimal compliance design and the optimal stress design have the same value of volume, 50%

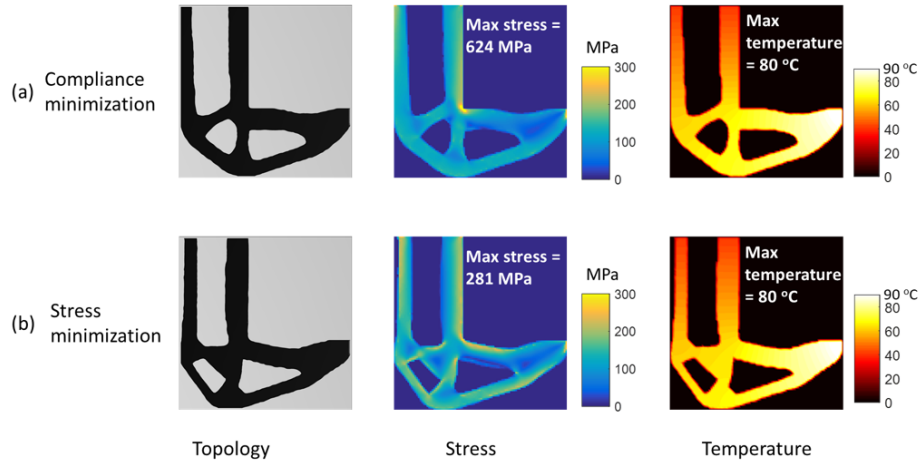


Figure 4: Optimal topologies obtained by minimizing structural compliance and stress. The stress plots are clipped at 300 MPa.

and the same maximum temperature, 80 °C. However, the optimal compliance design has a sharp re-entrant corner and as a result, a high value of maximum stress, 624 MPa. On the other hand, the optimal stress design has a rounded re-entrant corner and as a result, a low value of maximum stress, 281 MPa, which is a 55 % reduction in maximum stress. In conclusion, we can see that for the L-bracket example, minimizing compliance under a volume constraint and a maximum temperature constraint does not result in low values of stresses.

### 3.1.3. Mass minimization under stress and temperature constraints

The compliance minimization or stress minimization subject to a volume constraint is a common optimization formulation found in topology optimization literature. However, the mass minimization subject to stress and/or temperature constraints is a more prominent optimization formulation used by designers in industry. In this section, the mass minimization of the structure subject to constraints on the maximum stress and temperature is investigated. The temperature constraint  $T^* = 85^\circ\text{C}$  and the stress constraint  $\sigma^* = 300 \text{ MPa}$ . The obtained design is compared against the optimized design obtained by ignoring stress or temperature constraints, and the benefits of including both the

constraints, i.e., the advantages of using a multi-physics approach to solve this problem is discussed. The optimization problem can be described as

$$\begin{aligned}
& \min \rho V \\
& \text{subject to} \\
& K_t t = q_t \\
& K_s d = f_m + Ht \\
& \sigma \leq \sigma^* \\
& T \leq T^*
\end{aligned} \tag{45}$$

In Figure 5a, the minimum mass design subject to both stress and temperature constraints is shown. The optimized mass of the structure is 126 g, and the temperature and stress constraints are satisfied. In Figure 5b, the minimum mass design subject to only the stress constraint is shown. The optimal mass is 90 g, which is lower by 29% than the optimal mass obtained for the design with both stress and temperature constraints (126 g). For this case, the stress constraint is satisfied, but the maximum temperature is significantly high (113 °C). On the other hand, when the mass is minimized subject to only the temperature constraint, the optimal mass is 101 g, which is also lower by 20% than the optimal mass for design case with both stress and temperature constraints (126 g). For this case, the temperature constraint is satisfied, but the maximum stress of the structure is significantly high, 2252 MPa (a 650% increase).

In conclusion, this investigation shows that using a multi-physics approach for this problem, i.e, including both stress and temperature constraints in the optimization, yields a heavier design compared to the designs obtained using a single-physics approach, i.e, with ignoring stress or temperature constraints. However, the designs obtained by ignoring stress constraints have significantly higher values of stress, and the designs obtained by ignoring temperature constraints have significantly higher values of temperature, as one might expect.

To gain some mathematical understanding on why the multiphysics model yields a heavier design, we present a design space exploration study of a simple

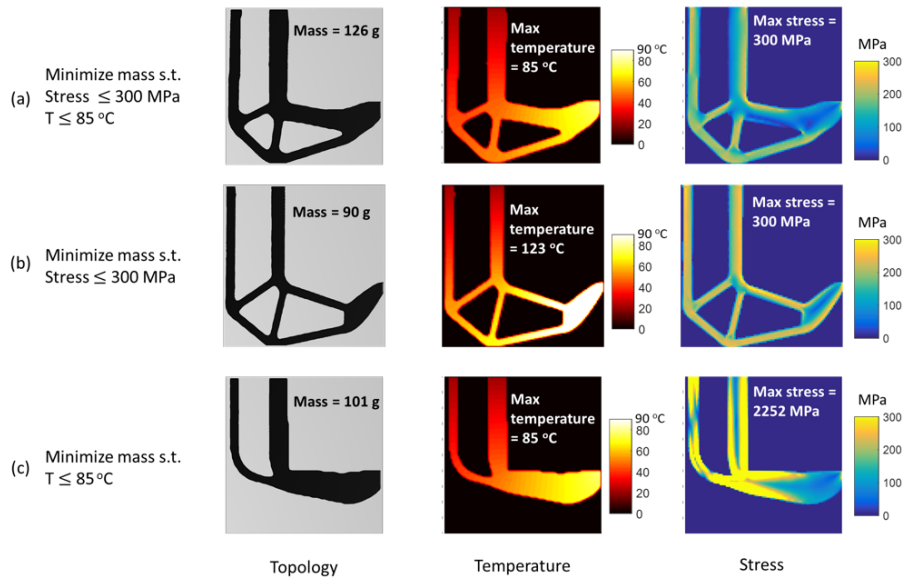


Figure 5: Minimum mass designs of the L-bracket subject to temperature and/or stress constraints. The stress plots are clipped at 300 MPa; while the temperature plots are clipped at 90 °C.

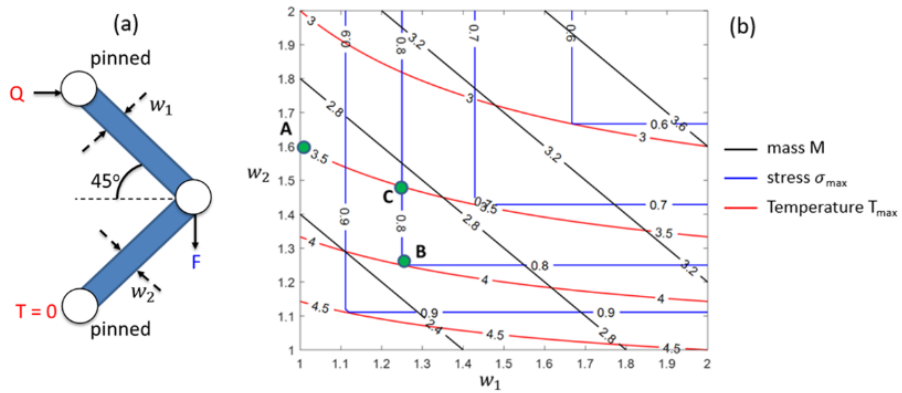


Figure 6: (a) Schematic of a two bar truss. (b) The iso-contours of mass, maximum stress and maximum temperature of a design study of the variables  $w_1$  and  $w_2$ .

two bar truss example as shown in Figure 6a. Both of the bars are pinned on the left side and a vertical force  $F$  is applied on the right side. The bar on the bottom (Bar-2) is attached to a heat sink ( $T = 0$ ) and a thermal load of  $Q$

is applied to the bar on the top (Bar-1). The bars are assumed to be having unit values for depth, length, density, and elastic modulus. The conductivity coefficient of Bar-1 and Bar-2 are 1 and 0.25, respectively. The design variables are the bar thicknesses  $w_1 \in [1, 2]$  and  $w_2 \in [1, 2]$ , as shown in Figure 6a. The analytical expressions for the maximum stress  $\sigma_{\max}$ , the maximum temperature  $T_{\max}$ , and the mass  $M$  of the two bar truss for  $F = \sqrt{2}$  and  $Q = 1$  are given by

$$\begin{aligned}\sigma_{\max} &= \frac{1}{\min(w_1, w_2)} \\ T_{\max} &= \frac{1}{w_1} + \frac{4}{w_2} \\ M &= w_1 + w_2\end{aligned}\tag{46}$$

Figure 6b shows the results of the design space exploration. Specifically, the iso-contours of the mass  $M$ , maximum stress  $\sigma_{max}$  and maximum temperature  $T_{max}$  for the design variables (the bar thicknesses)  $w_1 \in [1, 2]$  and  $w_2 \in [1, 2]$  are shown. In Figure 6b, the design point A  $((w_1, w_2) = (1, 1.6))$  which is the minimum mass design subject to a temperature constraint of  $T^* = 3.5$ , has a mass of 2.6. The design point B  $((w_1, w_2) = (1.25, 1.25))$  which is the minimum mass design subject to a stress constraint of  $\sigma^* = 0.8$ , has a mass of 2.5. The design point C  $((w_1, w_2) = (1.25, 1.48))$  which is the multiphysics based minimum mass design subject to both: a stress constraint of  $\sigma^* = 0.8$  and a temperature constraint of  $T^* = 3.5$ , has a mass of 2.73. In conclusion, this two bar truss example shows that the optimized multiphysics based design C has a higher mass (2.73) than the single physics based designs A and B (2.6 and 2.5). This is because the steepest gradients of the temperature and stress w.r.t. to the design variables  $w_1, w_2$  have different directions, which forces the optimizer to arrive at a heavier design for satisfying both the constraints.

### 3.2. Battery pack design

In this section, topology optimization of a battery pack under thermal and mechanical loading is presented. A schematic of a battery pack (dimensions are

20 cm  $\times$  20 cm  $\times$  5 cm) is shown in Figure 7. The structure is subjected to a uniform loading ( $F = 10^6$  N/m) on all four sides. Each battery cell (diameter of 2 cm) is assumed to be a non-designable non-load carrying member and it generates a thermal load of  $Q = 90$  W. The outer part of the structure is assumed to be acting as a heat sink, with  $T = 20$  °C. Due to the symmetry, only a quarter of the structure is modeled using an FEA mesh of  $100 \times 100$  elements. The elastic modulus of the structure is  $E = 69$  GPa and Poisson’s ratio  $\nu = 0.3$ , density  $\rho = 2700$  kg/m<sup>3</sup>, and thermal conductivity  $\kappa = 235$  W/m/°C. The reference temperature used is  $T_{ref} = 20$  °C.

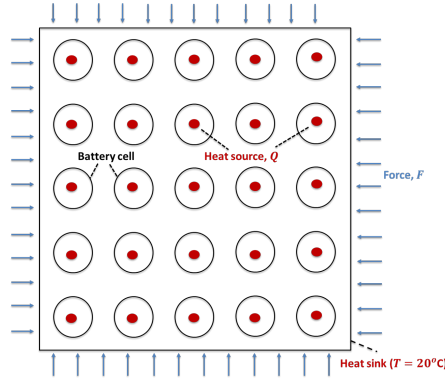


Figure 7: A schematic of a battery pack subject to mechanical and thermal loading.

### 3.2.1. Stress minimization

In this section, the p-norm stress of the structure is minimized subject to a volume constraint of 45%, for maximum temperature constraints from  $T^* = 50$ °C, 55°C, and 60°C, and the corresponding optimum topologies obtained are shown in Figure 8. In Figure 8a, the optimum design for a low value of a temperature constraint  $T^* = 50$  °C is shown. For this case, we can see that the optimum topology has a lot of material along the horizontal and vertical axes of symmetry of the structure. The battery cell at the center is the farthest from the heat sink, therefore the region around this battery cell is the hottest region. Therefore, for low values of the temperature constraints, the optimizer tries to minimize the thermal load path from the battery cell at the center to

the heat sink on the boundary—by adding material along the horizontal and vertical axes of symmetry. As a result, we can see that many regions of the structure are under high values of stress (regions in yellow in the stress plot), with the maximum stress being 136 MPa.

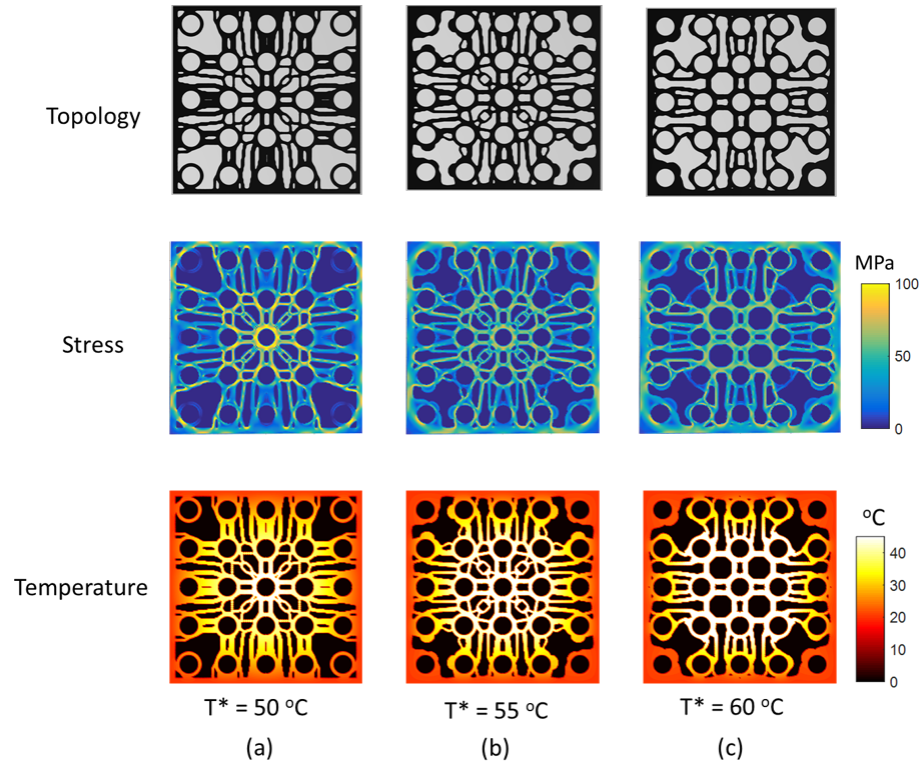


Figure 8: Optimal topologies, and the corresponding stress and temperature distributions obtained by minimizing the p-norm stress subject to a volume constraint of 45% and a range of maximum temperature constraints. The stress plots are clipped at 100 MPa and temperature plots are clipped at 45 °C.

In Figures 8b and 8c, the optimum designs for a temperature constraints of  $T^* = 55\text{ }^\circ\text{C}$  and  $T^* = 60\text{ }^\circ\text{C}$  is shown, respectively. From the figures, we can see that for increasing values of the temperature constraint, the optimizer removes material along the horizontal and vertical axes of symmetry and redistributes them so as to minimize stress while satisfying the temperature constraint. As a result, the maximum stress in the structure is reduced, with the maximum

stress values being 98.6 MPa and 97.7 MPa for the designs with a temperature constraint  $T^* = 55 \text{ }^\circ\text{C}$  and  $T^* = 60 \text{ }^\circ\text{C}$ , respectively. Clearly, the resulting maximum stress is highly sensitive to the maximum temperature constraint imposed.

### 3.2.2. Compliance minimization

In this section, the battery pack is designed by optimizing for compliance instead of stress. The obtained minimal compliant design is compared with the minimum stress design. Specifically, the compliance  $C$  of the battery pack is minimized subject to a volume constraint of 45% and a maximum temperature constraint of  $55 \text{ }^\circ\text{C}$ .

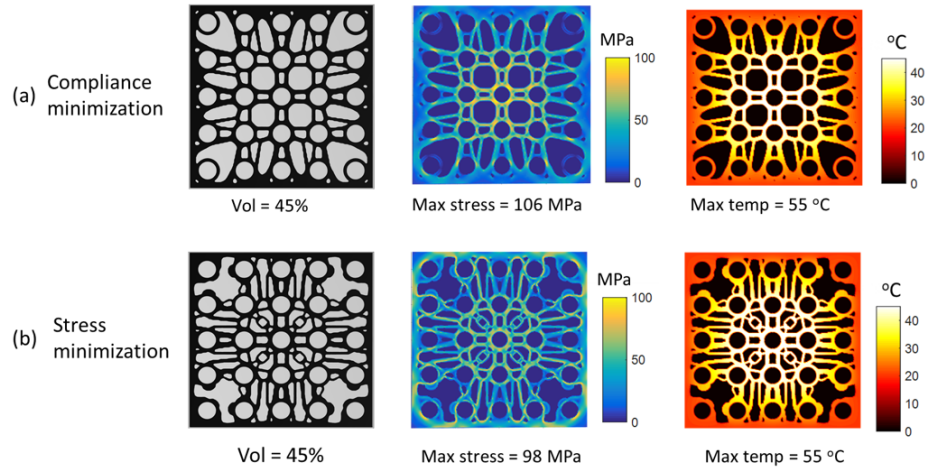


Figure 9: Optimal topologies obtained by minimizing structural compliance and stress. The stress plots are clipped at 100 MPa and temperature plots are clipped at  $45 \text{ }^\circ\text{C}$ .

Figure 9a shows the minimal compliant topology, and the corresponding stress and temperature distributions. For the sake of comparison, we show in Figure 9b the optimal topology and corresponding stress and temperature distribution of the minimal stress design subject to the same set of constraints (i.e, Figure 8b).

From Figure 9, we can see that the optimal compliant and stress designs have the same volume of 45% and same maximum temperature of  $55 \text{ }^\circ\text{C}$ . How-

ever, the minimal compliant design has a maximum stress of 106 MPa, while the minimal stress design has a maximum stress of 98 MPa, which is a 8% reduction in maximum stress. In conclusion, we can see that for this example, the optimal compliant design under a volume constraint and a maximum temperature constraint results in a higher value of stress (as one would expect), compared to the optimal stress design. Consequently, when performing an optimal compliant design, if the maximum stress exceeds the yield stress (or failure stress) of the material, the material can fail and negatively affect the heat dissipation properties of the battery pack, thus catastrophically triggering thermal runaway.

### 3.2.3. Mass minimization subject to stress and temperature constraints

In this section, the mass of the battery pack structure is minimized subject to the constraints on the maximum stress and temperature. The maximum temperature constraint  $T^* = 50^\circ\text{C}$  and the stress constraint  $\sigma^* = 100$  MPa. The obtained design is compared with the optimized design obtained by not including stress or temperature constraints, and the benefits of including both the constraints, i.e., the advantages of using a multi-physics approach to solve this problem is discussed.

The optimal design obtained subject to both stress and temperature constraints is shown in Figure 10a. The optimized mass of the structure is 2.51 kg and the temperature and stress constraints are satisfied. When the mass is minimized subject to only the stress constraint, the optimal mass 1.85 kg (Figure 10b), which is lower (by 26%) than the design case with both stress and temperature constraints (2.51 kg). The stress constraint is satisfied, but the maximum temperature is significantly high, i.e., 81 °C. On the other hand, when the mass is minimized subject to only the temperature constraint, the optimal mass is 2.38 kg (Figure 10c), which is also lower (by 5%) than the design case with both stress and temperature constraints (2.56 kg). The temperature constraint is satisfied, but the maximum stress of the structure is significantly higher, 273 MPa (a 173% increase over the multi-physics design in Figure 10a).

In conclusion, this investigation, similar to the L bracket design case, shows

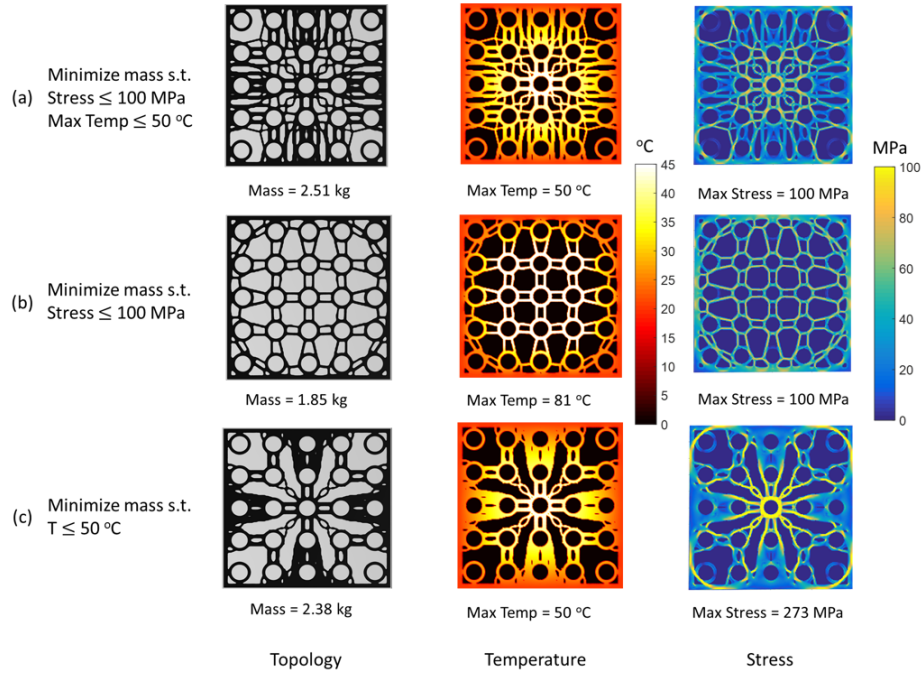


Figure 10: Minimum mass designs of the battery pack subject to temperature and/or stress constraints. The stress plots are clipped at 100 MPa and temperature plots are clipped at 45 °C.

the importance of using a multiphysics approach for solving this problem. Including both stress and temperature constraints, i.e., using a multi-physics approach in optimization yields heavier designs compared to the designs obtained using a single-physics approach, i.e., with ignoring stress or temperature constraints. Clearly, designs obtained by ignoring the stress constraints, yield stress states that are mechanically far from the optimum; whereas the designs obtained by ignoring temperature constraints are thermally far from the optimum—they have a significantly higher values of temperature.

Finally, we show the advantages of using the level set method for topology optimization. The structural boundary, which is implicitly and precisely defined by the level set function, can be readily represented as a CAD geometry model without any post-processing. For instance, the CAD model of the minimum

mass battery pack design subject to the stress and temperature constraints (Figure 10a) is shown in Figure 11.

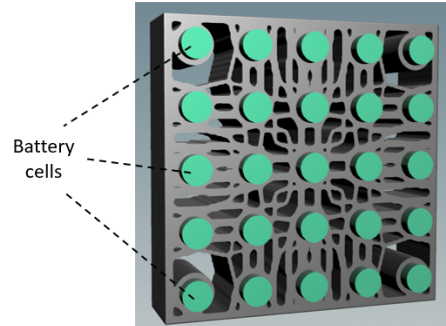


Figure 11: A CAD model of the lightweight battery pack optimized for stress and temperature.

#### 4. Conclusion

Topology optimization under coupled mechanical and thermal loads subject to stress and temperature constraints is presented in this paper. The investigation revealed that stress and temperature can be conflicting criteria in optimization. Specifically, the stress is decreased from 1000 MPa to 300 MPa, a 70% reduction, when the temperature constraint is increased from 70 °C to 90 °C for the L-bracket example. For the battery pack example, the stress is decreased from 136 MPa to 98 MPa, an 28% reduction, when the temperature constraint is increased from 50 °C to 60 °C.

Additionally, the designs obtained by minimizing compliance under temperature constraints do not necessarily have low stress values. Specifically, the optimal compliant L-bracket designed for a temperature constraint of 80 °C has a maximum stress of 624 MPa, while the L-bracket designed for stress has a maximum stress of 281 MPa, which amounts to a 55% reduction in stress. Similarly, the optimal compliant battery pack designed for a temperature constraint of 55 °C has a maximum stress of 106 MPa, while the battery pack designed

for stress under the same 55 °C temperature constraint has a maximum stress of 98 MPa, which amounts to a 8% reduction in stress.

Finally, the importance of using a multi-physics model—a coupled conduction and thermo-elastic model—in optimization is demonstrated. The designs obtained by minimizing mass under stress and temperature constraints are compared to the designs obtained by minimizing mass under only stress or only temperature constraints. It is found that the designs obtained under both of the constraints are heavier than the designs obtained under only one of the two constraints. However, the designs obtained under only temperature constraints have high values of stress; and the designs obtained under only stress constraints have high values of temperature. For example, the optimum mass of the L-bracket designed under only the temperature constraint is 20% lighter but has a maximum stress value that is 650% higher than the design obtained by including the stress constraint. Similarly, the optimal mass of the battery pack designed under only the temperature constraint is 5% lighter but has a maximum stress value that is 173 % higher than the design obtained by including both constraints. Thus, this demonstrates that the optimum stress and temperature values obtained using a single-physics model are quite far from the optimum stress and temperature values obtained using the multi-physics model.

Our results show that some members in the optimum designs are not under high values of stress, but they are necessary for satisfying the temperature constraint. Therefore, we believe that further design improvements may be achieved by judiciously replacing the material throughout the structure with highly conductive material in places where stresses are low to increase heat dissipation and/or in high stressed areas with higher strength material to minimize weight. Consequently, we believe that our methodology will facilitate Integrated Computational Materials Engineering (ICME), since it specifically enables integrating multi-physics considerations in the design as well as fit- for- purpose material design.

## Acknowledgments

The authors acknowledge the support from DARPA (Award number HR0011-16-2-0032) and NASA's Transformation Tools and Technologies Project (grant number 80NSSC18M0153). We also thank Dr. Steve Arnold at NASA Glenn for his insightful comments that greatly improved the manuscript.

## References

- [1] T. Dbouk, A review about the engineering design of optimal heat transfer systems using topology optimization, *Applied Thermal Engineering* 112 (2017) 841–854.
- [2] M. P. Bendsøe, Optimal shape design as a material distribution problem, *Structural optimization* 1 (4) (1989) 193–202.
- [3] N. P. van Dijk, K. Maute, M. Langelaar, F. Van Keulen, Level-set methods for structural topology optimization: a review, *Structural and Multidisciplinary Optimization* 48 (3) (2013) 437–472.
- [4] H. Rodrigues, P. Fernandes, A material based model for topology optimization of thermoelastic structures, *International Journal for Numerical Methods in Engineering* 38 (12) (1995) 1951–1965.
- [5] Q. Xia, M. Y. Wang, Topology optimization of thermoelastic structures using level set method, *Computational Mechanics* 42 (6) (2008) 837.
- [6] T. Gao, W. Zhang, Topology optimization involving thermo-elastic stress loads, *Structural and multidisciplinary optimization* 42 (5) (2010) 725–738.
- [7] P. Pedersen, N. L. Pedersen, Strength optimized designs of thermoelastic structures, *Structural and Multidisciplinary Optimization* 42 (5) (2010) 681–691.
- [8] J. D. Deaton, R. V. Grandhi, Stress-based design of thermal structures via topology optimization, *Structural and Multidisciplinary Optimization* 53 (2) (2016) 253–270.

- [9] J. Hou, J.-H. Zhu, Q. Li, On the topology optimization of elastic supporting structures under thermomechanical loads, *International Journal of Aerospace Engineering* 2016.
- [10] M. Takaloozadeh, G. H. Yoon, Development of pareto topology optimization considering thermal loads, *Computer Methods in Applied Mechanics and Engineering* 317 (2017) 554–579.
- [11] Q. Li, G. P. Steven, O. M. Querin, Y. Xie, Structural topology design with multiple thermal criteria, *Engineering Computations* 17 (6) (2000) 715–734.
- [12] N. de Kruijf, S. Zhou, Q. Li, Y.-W. Mai, Topological design of structures and composite materials with multiobjectives, *International Journal of Solids and Structures* 44 (22-23) (2007) 7092–7109.
- [13] T. Gao, P. Xu, W. Zhang, Topology optimization of thermo-elastic structures with multiple materials under mass constraint, *Computers & Structures* 173 (2016) 150–160.
- [14] Z. Kang, K. A. James, Multimaterial topology design for optimal elastic and thermal response with material-specific temperature constraints, *International Journal for Numerical Methods in Engineering* 117 (10) (2019) 1019–1037.
- [15] X. Zhu, C. Zhao, X. Wang, Y. Zhou, P. Hu, Z.-D. Ma, Temperature-constrained topology optimization of thermo-mechanical coupled problems, *Engineering Optimization* (2019) 1–23.
- [16] A. Takezawa, G. H. Yoon, S. H. Jeong, M. Kobashi, M. Kitamura, Structural topology optimization with strength and heat conduction constraints, *Computer Methods in Applied Mechanics and Engineering* 276 (2014) 341–361.
- [17] S. Deng, K. Suresh, Stress constrained thermo-elastic topology optimization with varying temperature fields via augmented topological sensitivity

- based level-set, *Structural and Multidisciplinary Optimization* 56 (6) (2017) 1413–1427.
- [18] J. A. Sethian, *Level set methods and fast marching methods: evolving interfaces in computational geometry, fluid mechanics, computer vision, and materials science*, Vol. 3, Cambridge university press, 1999.
- [19] J. A. Sethian, A. Vladimirov, Fast methods for the eikonal and related hamilton–jacobi equations on unstructured meshes, *Proceedings of the National Academy of Sciences* 97 (11) (2000) 5699–5703.
- [20] J. N. Reddy, D. K. Gartling, *The finite element method in heat transfer and fluid dynamics*, CRC press, 2010.
- [21] P. D. Dunning, H. A. Kim, Introducing the sequential linear programming level-set method for topology optimization, *Structural and Multidisciplinary Optimization* 51 (3) (2015) 631–643.
- [22] J. S. Arora, *Introduction to optimum design*, Elsevier, 2004.
- [23] P. D. Dunning, H. A. Kim, G. Mullineux, Investigation and improvement of sensitivity computation using the area-fraction weighted fixed grid fem and structural optimization, *Finite Elements in Analysis and Design* 47 (8) (2011) 933–941.
- [24] O. C. Zienkiewicz, R. L. Taylor, J. Z. Zhu, *The finite element method: its basis and fundamentals*, Elsevier, 2005.
- [25] C. Le, J. Norato, T. Bruns, C. Ha, D. Tortorelli, Stress-based topology optimization for continua, *Structural and Multidisciplinary Optimization* 41 (4) (2010) 605–620.
- [26] H. Lian, A. N. Christiansen, D. A. Tortorelli, O. Sigmund, N. Aage, Combined shape and topology optimization for minimization of maximal von mises stress, *Structural and Multidisciplinary Optimization* 55 (5) (2017) 1541–1557.

- [27] R. Picelli, S. Townsend, C. Brampton, J. Norato, H. Kim, Stress-based shape and topology optimization with the level set method, *Computer methods in applied mechanics and engineering* 329 (2018) 1–23.
- [28] J. Chin, S. L. Schnulo, T. Miller, K. Prokopius, J. S. Gray, Battery performance modeling on sceptor x-57 subject to thermal and transient considerations, in: *AIAA Scitech 2019 Forum*, 2019, p. 0784.